Quantum mechanical scattering investigation of the thermionic and field induced emission components of the dark current in quantum well infrared photodetectors

N. E. I. Etteh[a] and P. Harrison
Institute of Microwaves and Photonics, School of Electronic and Electrical Engineering, University of Leeds, LS2 9JT, United Kingdom

(Received 14 January 2002; accepted for publication 2 April 2002)

The thermionic emission and field induced emission components of the dark current in quantum well infrared photodetectors are investigated using a quantum mechanical scattering theory approach. Calculations are performed for an experimentally reported device. Using this as a standard, the device dimensions were altered in order to increase its detection wavelength to cover the mid- (MIR) and far-infrared (FIR) regions of the spectrum. The behavior of the scattering mechanisms that contribute to the thermionic emission and field induced emission components were studied. The results highlight the change in the dominating scattering mediator across the MIR and FIR bands. © *2002 American Institute of Physics.* [DOI: 10.1063/1.1481214]

I. INTRODUCTION

Quantum well infrared photodetectors (QWIPs) have recently attracted a lot of attention[1,2] due to their potential use as sensors in the far-infrared region (FIR) ($>14\ \mu$m).[3,4] Sensors in this region would be beneficial in the fields of astronomy, defense, and satellite mapping compared to their currently used counterparts, such as thermal and Ge detectors.[5,6] This is due to the high quality of materials used to make them and to the mature growth process.[7] However, extending the operating wavelength of QWIPs from the mid-infrared is difficult as the noise source of QWIPs, the dark current, inhibits the detection of these (expected) weak signals. The term ''dark current'' refers to the flow of electronic charge in the device without the presence of incident light. Practical attempts to reduce the dark current has been limited to cooling of the device.[1,8–10] and to the development of different QWIP structures, for example, with double barriers.[11]

There are three physical mechanisms that contribute to the dark current, and these are described in Fig. 1. The ground state sequential tunnelling (ST) component involves electrons scattering from the localized state in one quantum well into the next. The thermionic emission (TE) component refers to the excitation of carriers from the well and into the continuum. The final component is called field induced emission (FIE) (or thermally assisted tunnelling), in which the thermalized carriers in the higher momentum states of the quantum well tunnel through the barrier tip and into the continuum. These processes occur under the influence of an applied field. Thus, once in the continuum, the carriers will constitute a current: the dark current.

To enable a reduction of the dark current by careful design in QWIPs, many physical models have been developed,[10,12,13] which predict the behavior of the dark current for given QWIP device parameters. However, for a more accurate prediction of the dark current in QWIPs, a quantitative microscopic model is necessary.[12,14,15] In a previous work,[15] quantum mechanical calculations of the dark current focused on the sequential tunnelling component. Recently reported new approaches to the thermionic emission component have been limited to qualitative predictions with a simple model.[16,17]

The relative contribution of each of the components to the total dark current has not been explored, however. In being able to understand the physics of each component (for example, the most dominating scattering mechanism in each component at a certain temperature), steps can be made toward a full quantitative microscopic quantum mechanical model of the dark current. With this aim, this work focuses on the physics of the TE and FIE components of the dark current in QWIPs. The ST component is generally neglected in device physics, assumed to be a negligible value when compared to the other components,[1,14,18,19] and previous work justifies this.[20,21]

II. THEORETICAL APPROACH AND METHODS

The theoretical techniques and numerical methods used in this paper are based on the one-dimensional Schrödinger equation for an electron within a heterostructure semiconductor, and under the influence of an electric field F, as shown below:

$$\left[-\frac{\hbar^2}{2}\frac{\partial}{\partial z}\frac{1}{m^*(z)}\frac{\partial}{\partial z}+V(z)-eFz\right]\psi(z)=E\psi(z), \qquad (1)$$

where $\psi(z)$ is the wave function representing the particle under the effective mass and envelope function approximations, and z is the distance along the growth axis. A shooting method was used to solve the equation numerically to obtain the eigenfunction [$\psi(z)$] and eigenvalues (E). This information was then used to obtain the Fermi–Dirac distribution function for a given electron density.

[a]Electronic mail: eenneie@leeds.ac.uk

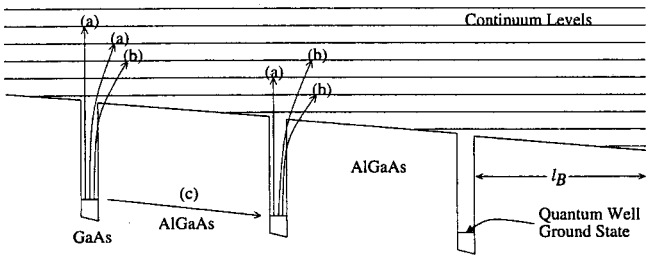

FIG. 1. Three mechanisms of the dark current: (a) thermionic emission, (b) field induced emission, (c) sequential tunnelling.

Using an approach based on Fermi's golden rule and the Born approximation, the wave functions were used to calculate the mediators of the dark current: electron–electron ($e-e$) and electron–longitudinal optical ($e-$LO) phonon scattering rates[14,15,22] (see Harrison [23] for full derivation and computer source code). Thermalized electron distributions were assumed, with the electron temperature taken equal to the lattice temperature.

A single rate for each transition was obtained by averaging both scattering mechanisms over these thermalized subband populations. The $e-e$ scattering mechanism, as a two-body problem, was calculated as the sum of its three different components, as described in Fig. 2.

As mentioned earlier, some interesting features have already been deduced with a simplistic model of the thermionic emission component of the dark current.[15] However, in order to improve the predictive qualities, it is desirable to quantify that model and also to include the contribution of field induced emission. To achieve this, consider discretizing the continuum as in Fig. 1. The total scattering from the well to the continuum would represent both the TE and FIE components, as shown in the figure. This was evaluated by summing the scattering rates over the continuum states c of increasing energy until convergence was achieved. Assuming that the quantum well ground state is labeled "1," the total scattering rates out of the well are given by:

$$\frac{1}{\tau^{e-\mathrm{LO}}}=\sum_{c=2}^{\infty}\frac{1}{\tau_{1,c}^{e-\mathrm{LO}}}, \tag{2}$$

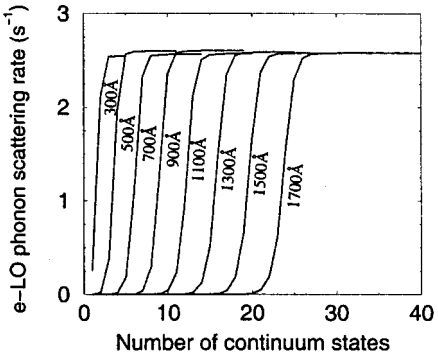

FIG. 3. An example of the total $e-$LO phonon absorption scattering rate from the bound state in a quantum well to the continuum as a function of the number of continuum states included in the summation at 77 K and for a variety of outer barrier widths.

$$\frac{1}{\tau^{e-e}}=\sum_{c=2}^{\infty}\frac{1}{\tau_{1,c}^{e-e}}. \tag{3}$$

The summation was controlled by increasing the outer barrier width (l_B) (see Fig. 1) for both $e-$LO phonon and $e-e$ scattering, i.e., the larger l_B, the more the number of continuum states involved in the summation. Figures 3 and 4 show the results of the calculations for a subband electron density in the quantum well of 10^{10} cm^{-2} and a bias of 3 V, which are typically used in QWIPs.

It can be seen that the summations converge for both $e-$LO and $e-e$ scattering independently of how the continuum is discretized (i.e., the number of states forming the continuum). This is important evidence to validate this approach: provided convergence is always obtained, the scattering rate is not sensitive to the number of continuum states.

III. MODELING AT DIFFERENT DETECTION WAVELENGTHS

In order to deduce the dominating mechanisms in the TE and FIE combination, three QWIP devices were modeled. These were of different detection wavelengths, based on a QWIP developed by Walther *et al.*[2] (44 Å GaAs quantum well separated by 470 Å $Ga_{0.63}Al_{0.27}As$ barriers), with a sheet carrier density in each well of $n=7.6\times10^{10}$ cm^{-2}.

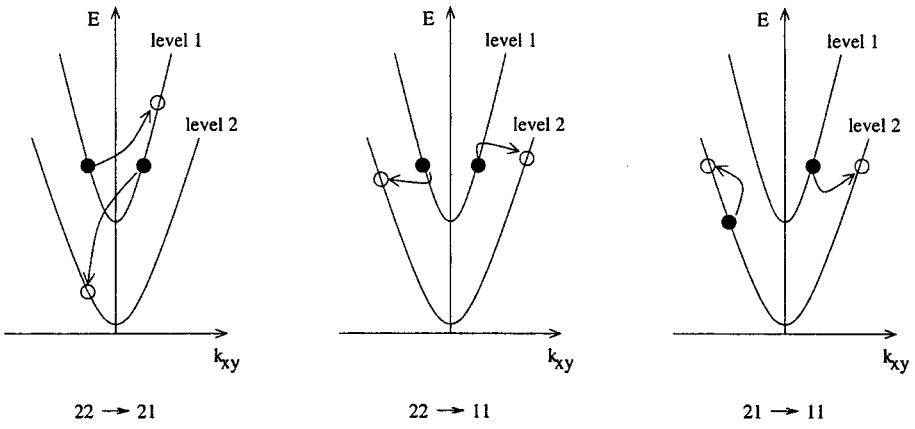

FIG. 2. Intersubband carrier–carrier scattering mechanisms in a two-level system (after Harrison Ref. 23): the solid circles represent the initial electron states, and the empty circles, the final states.

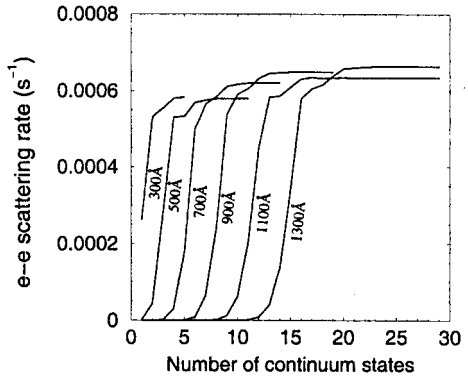

FIG. 4. An example of the total $e-e$ scattering rate from the bound state in a quantum well to the continuum as a function of the number of continuum states included in the summation at 77 K and for a variety of outer barrier widths (as indicated on the figure).

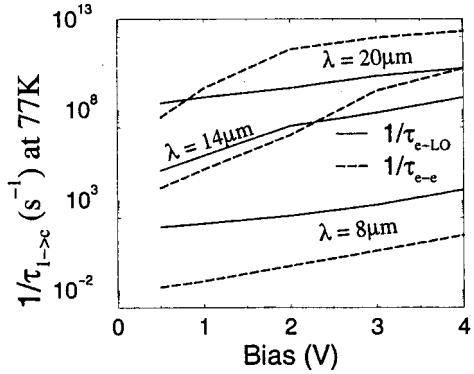

FIG. 6. Total $e-e$ and $e-$LO phonon absorption scattering rate from the quantum well to the continuum states as a function of detection wavelength for a temperature of 77 K.

With 20 quantum well periods, the distance between contacts (QWIP length) was 1.075 μm. The device dimensions are given as 37×37 μm^2, and the peak detection wavelength obtained was 8.1 μm. For detection wavelengths of 14 and 20 μm, well widths of 25 and 14 Å, respectively, were used (equivalent QWIP lengths of 1.037 and 1.015 μm, respectively), with all other parameters remaining constant. The results obtained are shown and discussed in the following sections.

A. Total scattering rate with respect to bias

The total $e-e$ and $e-$LO phonon scattering rates from the quantum well ground state to the continuum states are shown in Figs. 5 and 6, with respect to bias, at 65 and 77 K, respectively.

From the figures, it can be seen that $e-$LO phonon scattering dominates at low detection wavelengths ($\lambda=8$ μm). However, as the wavelength is increased, $e-e$ scattering increases in prominence. This occurs at a lower bias with increasing wavelength (i.e., $\approx$2 V for $\lambda=14$ μm, and $\approx$0.75 V for $\lambda=20$ μm). While the reason is unknown, it may be that this effect forces the low bias operation of high detection wavelength devices, as for example, in the device developed by Perera *et al.*[8] An increase in temperature results in an increase in the scattering rates, the qualitative characteristics remaining unchanged.

B. Total scattering rate with respect to detection wavelength

As the authors are motivated by the desire for FIR devices, the variation of the scattering rate with increasing wavelength is particularly appealing. This is shown in Figs. 7 and 8, as a function of bias.

For both 65 and 77 K, and at a low bias of 0.5 V, $e-$LO phonon scattering is the dominant mediator of scattering out of the well, regardless of detection wavelength. Once the bias starts to increase, however, $e-e$ scattering begins to dominate.

Most QWIP devices are operated at a bias between 2 and 3 V and at 77 K.[2,24–28]. Figure 8 shows that the highest detection wavelength at which $e-$LO phonon scattering dominates in this bias region is around 13.5 μm. This tends to be the highest peak detection wavelength of these devices. Thus, it seems there are two indications (the low bias voltage operation of long wavelength devices and the peak detection wavelength of typical biased devices) which suggests that successful QWIPs operate in regions were $e-e$ scattering is

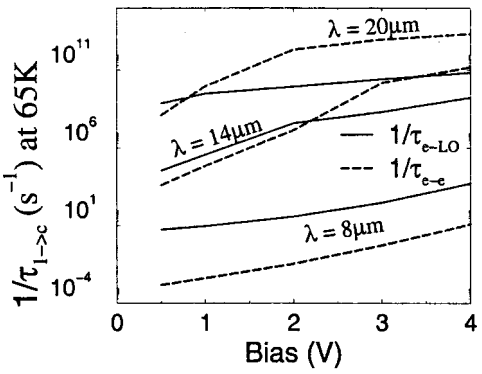

FIG. 5. Total $e-e$ and $e-$LO phonon absorption scattering rates from the quantum well to the continuum states as a function of detection wavelength for a temperature of 65 K.

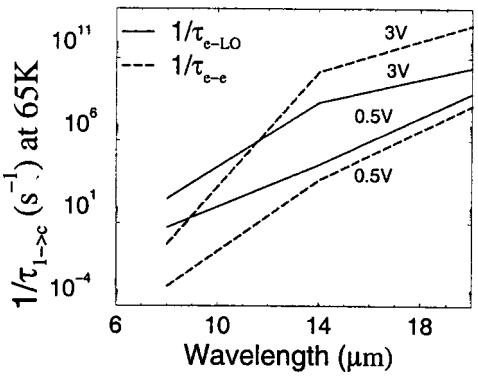

FIG. 7. Total scattering rate from the quantum well to the continuum states as a function of bias for both $e-e$ and $e-$LO phonon absorption scattering rates at a temperature of 65 K.

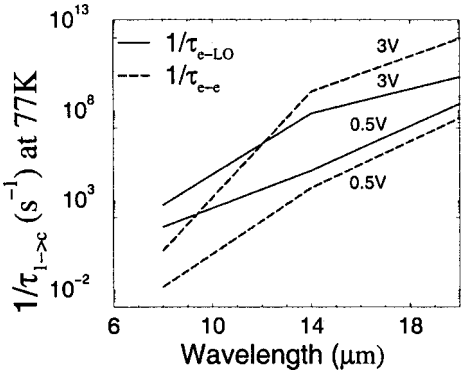

FIG. 8. Total scattering rate from the quantum well to the continuum states as a function of bias for both $e-e$ and $e-$LO phonon absorption scattering rates at a temperature of 77 K.

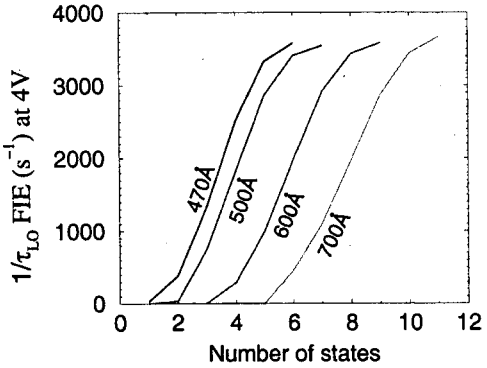

FIG. 10. Total $e-$LO phonon absorption scattering rate from the quantum well bound state to the continuum states as a function of the number of continuum states in the summation at 77 K, for four outer barrier widths at a bias of 4 V for the FIE component.

not dominating. The reasons for this are unknown at this time, but it could be used as a rule of thumb in future device design.

Hence, increasing the detection wavelength, may require reducing the doping density of the quantum wells in order to reduce the $e-e$ scattering rate. However, the re-sponsivity, and hence the detectivity, of the device may be undermined, depending on the amount of carriers in the well.[1,13,18] Thus, designers have the task of creating a compromise between detectivity and the dark current.

IV. RATIO OF FIE COMPONENT TO TOTAL DARK CURRENT WITH INCREASE IN BIAS

Having observed the behavior of the combined FIE and TE components with changes in bias and wavelength, it is interesting to know the relative sizes of these two effects. This was achieved by comparing the discretized continuum energy levels to the energy level of the barrier tip. The FIE component would account for electrons scattered to energy levels lower than the barrier tip, where tunneling through the barrier would have to occur, whereas those higher than the barrier tip would represent the TE component (see Fig. 9).

Figures 10 and 11 show the change in the FIE and TE components for the Walther *et al.* device[2] at 77 K (the operational temperature of the device). The figures focus on the $e-$LO scattering rate (which dominates over $e-e$ scattering, as shown in Fig. 6), with changes in the barrier width (which controls the energy and number of continuum levels) at 4 V bias.

It can be seen that convergence for different outer barrier widths, l_B, still occurs in the $e-$LO scattering rate characteristic for FIE (Fig. 10), as first described in Sec. II. However, the $e-$LO scattering rate characteristic for TE (Fig. 11) is erratic, but expected. This is due to the fact that with an increase in barrier width, energy levels formerly associated with TE move to a level below the barrier tip. This is a step function, and when it occurs, the scattering rate to energy levels above the well is obviously reduced.

Finally, the ratio of the FIE component to the total scattering rate out of the well (FIE and TE) with changes in bias, is shown in Fig. 12. The variation of this ratio with different outer barrier widths, l_B, is negligible ($<10\%$), further validating the model. It can be seen from the figure that the FIE component does become the dominant component of the dark current, as the bias is increased. This has been speculated many times before e.g.,[1,18] but proven here theoretically, for the first time. Calculations show that the erratic convergence behavior of the TE component shown earlier does not affect this FIE total-dark-current ratio.

V. CONCLUSION

A detailed, first principles, quantum mechanical representation of the thermionic emission and field induced emis-

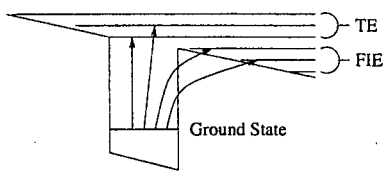

FIG. 9. Schematic of the FIE and TE components of the dark current with respect to the barrier tip.

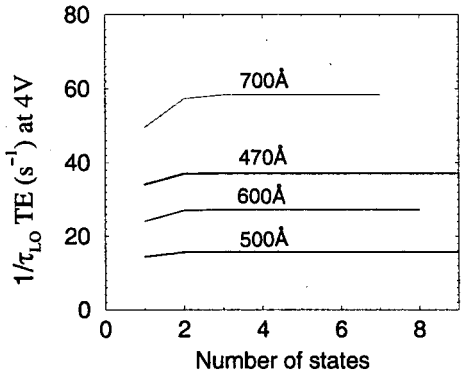

FIG. 11. Total $e-$LO phonon absorption scattering rate from the quantum well bound state to the continuum states as a function of the number of continuum states in the summation at 77 K for four outer barrier widths at a bias of 4 V for the TE component.

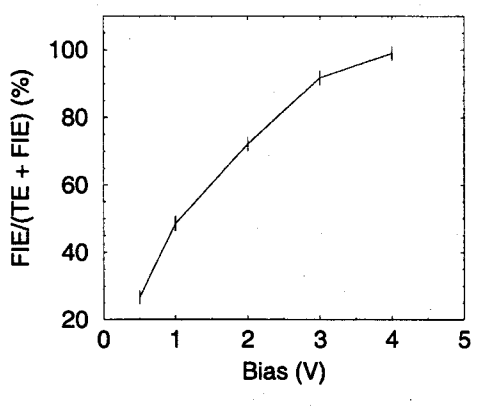

FIG. 12. Ratio of FIE component to total dark current in a QWIP with respect to change in bias, ratio error bars illustrated.

sion components of the dark current in QWIPs has been developed, based on calculations of phonon and carrier–carrier scattering in QWIPs.

The results give insight into the bias, detection wavelength, and temperature dependencies of the thermionic and field induced emission components of the dark current. It has been shown that as the detection wavelength is increased, electron–electron scattering plays a greater role in the dark current of QWIPs. The relative strengths of the FIE and TE components have been calculated for the first time. The results show that the FIE component dominates exclusively at biases of around 4 V for a device reported in the literature.

ACKNOWLEDGMENTS

The authors would like to acknowledge financial support from the School of Electronic and Electrical Engineering, and discussions with E. H. Linfield of the University of Cambridge.

[1] B. F. Levine, J. Appl. Phys. **74**, R1 (1993).
[2] M. Walther *et al.* in *Intersubband Transitions in Quantum Well: Physics and Devices*, edited by Sheng S. Li and Yan-Kuin Su (Kluwer Academic, Boston, 1998).
[3] J. M. Chamberlain and R. E. Miles, *New Directions in Terahertz Technology*, (Kluwer, Dordecht, 1997).
[4] *IEEE Sixth International Conference on Terahertz Electronics Proceedings*, edited by P. Harrison (Institute of Electronics and Electrical Engineers, Piscataway, NJ, 1998).
[5] Antoni Rogalski, Proc. SPIE **2**, 754 (1998).
[6] S. D. Gunapala and S. V. Bandara, *Intersubband Transitions in Quantum Well: Physics and Device Applications I*, edited by H. C. Liu and F. Capasso, (Academic, San Diego, 2000).
[7] Walter R. Dyer and Meimei Z. Tidrow, Proc. SPIE **3379**, 434 (1998).
[8] A. G. U. Perera, S. G. Matsik, H. C. Liu, M. Gao, M. Buchanan, W. J. Schaff, and W. Yeo, Appl. Phys. Lett. **77**, 741 (2000).
[9] A. Rogalski, Infrared Phys. Technol. **40**, 279 (1999).
[10] C. J. Chen, K. K. Choi, L. Rokhinson, W. H. Wang, and D. C. Tsui, Appl. Phys. Lett. **75**, 3210 (1999).
[11] B. F. Levine, A. Zussman, S. D. Gunapala, M. T. Asom, J. M. Kuo, and W. S. Hobson, J. Appl. Phys. **72**, 4429 (1992).
[12] H. C. Liu, A. G. Steele, M. Buchanan, and Z. R. Wasilewski, J. Appl. Phys. **73**, 2029 (1993).
[13] H. C. Liu, in *Intersubband Transitions in Quantum Well: Physics and Device Applications I*, edited by H. C. Liu and F. Capasso (Academic, San Diego, 2000).
[14] J. Y. Andersson, J. Appl. Phys. **78**, 6298 (1995).
[15] N. E. I. Etteh and P. Harrison, IEEE J. Quantum Electron. **37**, 672 (2001).
[16] M. A. Gadir, P. Harrison, and R. A. Soref, MSS10 Conference, July, 2001, Linz, Austria [Physica E (to be published)].
[17] M. A. Gadir, P. Harrison, and R. A. Soref, Superlatt. Microstruct **30**, 135 (2001).
[18] R. L. Whitney, K. F. Cuff, and F. W. Adams, in *Semiconductor Quantum Wells and Superlattices for Long-Wavelength Infrared Detectors*, edited by M. O. Manasreh (Artech House, Boston, 1993).
[19] S. Gunapala, G. Sarusi, J. Park, T. Lin, and B. F. Levine, Phys. World **7**, 35 (1994).
[20] N. E. I. Etteh and P. Harrison, MSS10 Conference, July, 2001, Linz, Austria, [Physica E (to be published)].
[21] N. E. I. Etteh and P. Harrison, Superlatt. Microstruct. (to be published).
[22] O. Madelung, *Introduction to Solid-State Theory* (Springer, Berlin, 1978).
[23] P. Harrison, *Quantum Wells, Wires and Dots: Theoretical and Computational Physics* (Wiley, Chichester, 1999).
[24] B. F. Levine, C. G. Bethea, G. Hasnain, V. O. Shen, E. Pelve, R. R. Abbott, and S. J. Hsieh, Appl. Phys. Lett. **56**, 851 (1990).
[25] A. Zussman, B. F. Levine, J. M. Kuo, and J. de Jong, J. Appl. Phys. **70**, 5101 (1991).
[26] Y. Fu, Ning Li, M. Karlsteen, M. Willander, Na Li, W. L. Xu, W. Lu, and S. C. Shen, J. Appl. Phys. **87**, 511 (2000).
[27] S. D. Gunapala, J. S. Park, G. Sarusi, T. Lin, J. K. Liu, P. D. Maker, R. E. Muller, C. A. Shott, and T. Hoelter, IEEE Trans. Electron Devices **44**, 45 (1997).
[28] M. Z. Tidrow, Mater. Sci. Eng., B **74**, 45 (2000).